A New Polymorph of *N*,*N*′-Dimethylurea Characterized by X-ray Diffraction and First-Principles Lattice Dynamics Calculations

David. M. S. Martins,[†] Christopher K. Spanswick,[†] Derek S. Middlemiss,[‡] Nasir Abbas,[†] Colin R. Pulham,[†] and Carole A. Morrison*,[†]

School of Chemistry and EaSTCHEM Research School, The University of Edinburgh, King's Buildings, West Mains Road, Edinburgh EH9 3JJ, U.K., and Department of Chemistry and WestCHEM Research School, University of Glasgow, University Avenue, Glasgow, U.K. G12 8QQ

Received: January 7, 2009; Revised Manuscript Received: March 24, 2009

In this study we present a combined crystallographic and computational study of a new polymorph of *N*,*N*′-dimethylurea (DMU) with $P2_12_12$ space group symmetry, along with a revised theoretical study of the previously known phase in its corrected space group (*Fdd*2). X-ray diffraction studies show crystal structures that are very similar, differing only in the relative orientation of the hydrogen-bonded molecular chains that are common to both phases. The vibrational spectra were obtained from B3LYP hybrid functional lattice dynamics calculations and compared with the experimental data for the known phase. The free-energy difference between the forms is derived from the Γ-point optical mode frequencies, and amounts to less than 1 kJ mol^{-1} across the temperature range of interest. The electronic densities-of-states of both phases are also computed, yielding only marginal differences in valence and conduction band compositions and band gap widths. Taken together, the results highlight the small but important differences separating the two crystal lattices.

I. Introduction

The defining ability of a molecular crystal to adopt more than one packing arrangement is a phenomenon of enduring interest in materials science and chemistry.[1] The generally weak intermolecular interactions often allow for facile molecular rearrangement, and the different polymorphs that emerge influence many of the chemical and physical properties of the material,[2] such as nonlinear optical (NLO) activity. However, differences in lattice energies between structures can often differ by only a few kJ mol^{-1},[3] thus rendering both the rational design (or "crystal engineering") and the theoretical study of such materials a challenge. Nevertheless, combined experimental and theoretical studies of molecular solids are now quite common in the literature;[4−6] their abundance testifies to the potential of such approaches to disclose many properties of interest in such materials. The present work falls within this broad class of approach, applying X-ray crystallography, Raman spectroscopy, and first-principles calculations to the study of a polymorphic disubstituted urea.

Compounds based on urea possess the ability to form a diverse range of hydrogen-bonded networks and constitute an important series of precursors in crystal engineering applications.[7−9] Urea in form I (see Figure 1a) presents a structure in which each molecule donates two hydrogen bonds to the carbonyl group of a neighboring unit forming one dimensional chains.[10] Neighboring chains alternate in the direction of orientation of their respective carbonyl groups, and as a consequence, the lattice is nonpolar. Symmetrically disubstituted ureas tend to adopt the same characteristic packing motif.[8,9,11−14]

The current study focuses on the compound *N*,*N*′-dimethylurea (DMU), which represents one of the simplest examples of a disubstituted urea. Alongside NLO applications, it has been shown to be of relevance within a wide variety of scientific and industrial processes (e.g., in membrane transport within red blood cells and as a stabilizer in hydrated lubricating oils).[15,16] The first account of the determination of the crystal structure dates back to 1924,[17] although this study is not entered in the

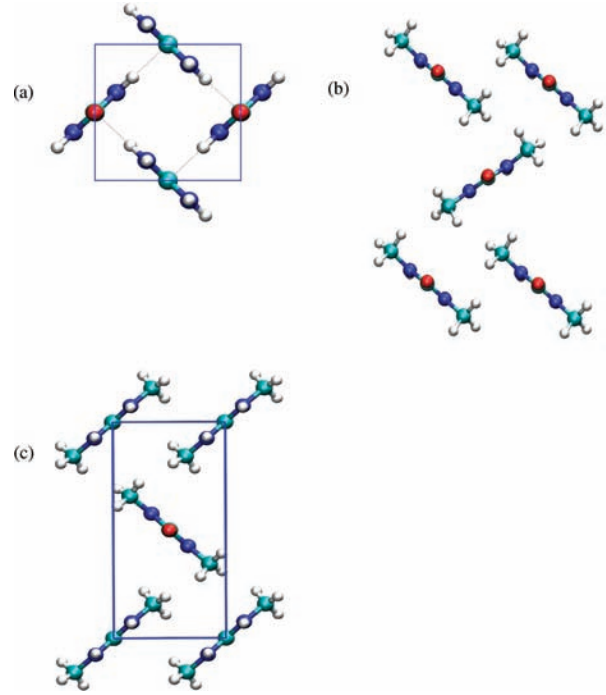

Figure 1. Projections onto the *ab*-plane of the (a) phase I urea, (b) phase I DMU, and (c) phase II DMU structures. Note that molecules stack via hydrogen bonding along the *c*-vector to create one-dimensional chains; for phase I urea and phase II DMU, neighboring chains pack in opposite directions, giving rise to nonpolar lattices. Neither DMU phase I nor II features hydrogen bonds in the *ab*-plane.

* To whom correspondence should be addressed. E-mail: Carole.Morrison@ed.ac.uk.
[†] The University of Edinburgh.
[‡] University of Glasgow.

10.1021/jp900141q CCC: $40.75
Published on Web 04/29/2009

Cambridge Structural Database (CSD).[18] Pérez-Folch et al. are generally credited with the first structural determination of DMU; their structural refinement assigned it to the *Cc* space group.[19] This result was unexpected for it indicated a polar structure, in contrast with that of the parent compound urea (Figure 1b). The authors also attempted a refinement in the *Fdd*2 space group but dismissed it on the basis that it led to larger thermal parameters and higher *R*-factors. Various crystallization techniques were applied in an effort to obtain a polymorph with packing more akin to that observed in urea, but these were all unsuccessful.[19] In fact, the crystalline symmetry of DMU was subsequently reassigned to the orthorhombic *Fdd*2 group by Marsh[20] during a survey of the CSD.

Recent work in our laboratory has now led to the discovery of this new polymorph (hereafter denoted as phase II), which should also be considered as a candidate NLO material. In addition to a full set of crystallographic details, we also report upon extensive computational studies, the aims of which were to determine the difference in free energies of the two polymorphs, to compare the details of their electronic structures, and to analyze the solid-state vibrational spectra. This last objective follows on from the previous work of Keuleers et al. on phase I within the erroneous *Cc* space group, in which the normal modes of a cluster of 15 molecules surrounded by 6048 point charges were obtained at the RHF/6-31++G** level.[21] The vibrational frequencies obtained in this fashion were then transformed into a symmetry coordinate force field and subsequently scaled against the experimental data. The present theoretical approach differs in that we perform lattice dynamics calculations within full periodic boundary conditions employing the B3LYP hybrid density functional,[22,23] which has previously been shown to provide accurate frequencies without recourse to scaling and at a reasonable computational cost.[24−26] We also calculate anharmonic corrections for selected C−H and N−H stretching motions.

II. Experimental and Computational Methods Section

i. Sample Preparation. Phase II was first obtained accidentally by means of slow evaporation (∼6 months) from a concentrated solution of DMU in aqueous phosphoric acid (∼5 M). Crystals of this phase were subsequently identified in samples of DMU purchased directly from Sigma-Aldrich.

ii. X-ray Diffraction. Studies of the colorless block-shaped crystals were undertaken using a Bruker-Smart Apex CCD diffractometer equipped with an Oxford Cryosystems low-temperature device operating at 150 K, employing Mo Kα radiation ($\lambda = 0.71073$ Å). Data reduction was performed using the program SAINT (Bruker Nonius).[27] An absorption correction was applied using the multiscan procedure program SADABS.[28] The structure was solved by direct methods using the SIR92[29] package and refined using a full-matrix least-squares algorithm against $|F|^2$ in the CRYSTALS program.[30] All atoms other than hydrogen were refined with anisotropic thermal parameters. Hydrogen atoms were placed geometrically and allowed to regularize with respect to Fourier difference peaks.

Crystal Data. Phase II: $C_3H_8N_2O$, 150 K, $M = 88.11$ g/mol, orthorhombic, space group $P2_12_12$ with $a = 4.9790(9)$, $b = 10.775(2)$, $c = 4.5764(9)$ Å, $Z = 2$, $V = 245.52(8)$ Å^3, $\rho_{calc} = 1.19$ g.cm^{-3}, and $R = 0.048$ (Rw = 0.098) for 395 independent reflections. The crystal selected was a colorless block of dimensions $0.31 \times 0.28 \times 0.22$ mm.

iii. Theoretical Basis. Geometry optimizations and lattice dynamics calculations were performed for both the new and previously reported polymorphs of DMU[19,20] within the CRYSTAL06 code.[31] Electronic exchange and correlation were included approximately by use of the B3LYP[22,23] hybrid density functional, while the crystalline orbitals were expanded in terms of standard, atom-centered 6-311G** Gaussian basis sets.[32] The SCF total energy convergence tolerance was set at 10^{-9} au, while the reciprocal space zone was sampled upon a Monkhorst−Pack mesh with a shrinking factor of 6.[33] Optimizations were pursued to a total energy convergence of 10^{-9} au, with rms gradient and displacement tolerances of 3×10^{-5} and 1.2×10^{-4} au, respectively. The tolerances for individual components of the gradients and displacements were set at 1.5 times the respective rms criterion. The harmonic vibrational normal modes of the lattices were obtained at the Γ-point for it is at this wavevector alone that phonons couple to the electric field of the impinging probe radiation in IR and Raman spectroscopies. The mass-weighted Hessian matrix was obtained from the numerical differentiation of the analytical gradient with respect to the atomic coordinates. Subsequent diagonalization of this matrix yields the frequencies (i.e., the eigenvalues) and atomic displacement patterns (i.e., the eigenvectors) of the normal modes of each lattice. Full details of the method and of the influence of the various computational parameters upon the computed frequencies have been presented within previous studies.[25,34]

The Hessian matrix was determined from a series of separate calculations in which individual atoms were translated by distances of 0.003 Å along the Cartesian axes. The filling of the matrix takes advantage of the lattice symmetry, so that only an irreducible set of atomic displacements need be explicitly considered. In the primitive cells of both phases, this entails shifts in the *x*-, *y*-, and *z*-directions of each of the atoms in the irreducible fragment of a single molecule (i.e., $CONHCH_3$), amounting to 24 displacements in total. The temperature-dependent harmonic free energies of the lattices were then obtained from the set of oscillator frequencies by the usual statistical mechanical analysis. We note that this approach neglects not only the dispersions in the optical modes, which are expected to be small in a molecular crystal, but also the dispersions in the acoustic modes, which are likely to be more substantial. While the missing contributions would be expected to largely cancel in considering the difference in the free energies of the two forms, we obtain more quantitative results by application of the Debye model,[35] parametrized in terms of the densities and bulk moduli of both phases. Since the latter values are unknown and cannot be readily accessed by the present calculations due to the poor representation of weak interactions, we proceed upon the assumption that they are both equal to the experimentally determined bulk modulus of phase I urea of 10.8 GPa.[36] The density-dependent specific internal energies of the acoustic motions, *U*, are obtained as

$$\frac{U}{Nk_B} = 3TD_3\left(\frac{T_D}{T}\right)$$

where *N* denotes the number of molecules, *T* the temperature, D_3 the third-order Debye function, and T_D the Debye temperature

$$T_D = \frac{h\bar{c}_S}{2k_B}\sqrt[3]{\frac{6N}{\pi V}}$$

where $\bar{c}_S$ is the mean acoustic velocity and *V* the volume occupied by the solid. The acoustic velocity is derivable from the bulk modulus and density by application of elasticity theory. Given the experimental densities of the phases, we obtain differences in the internal energies varying from 10^{-4} to 10^{-3}

kJ mol^{-1} across the range of temperatures from 20 to 400 K, which can be safely neglected. The limitations of this model are however clear, and our future work on polymorphic molecular crystals will consider thermodynamic functions obtained from the explicit integration of the phonon dispersion curves over the whole Brillouin zone. We note also that vibrational modes involving hydrogen atoms are prone to significant anharmonicity. We address this point for the stretching motions by solving a series of one-dimensional Schrödinger equations with potentials derived from sixth-order polynomial fits to total energies obtained over a range of N−H and C−H bond lengths. Two approaches were utilized for the N−H bonds, allowing us to either conserve or break the space group symmetry, whereas the C−H bond displacements all preserved the full lattice symmetry and thereby corresponded to the totally symmetric stretching mode.

Finally, plots of the electronic densities-of-states (DOS) of the two forms were obtained from the final density matrices at convergence and partitioned via the Mulliken method into separate O, C, N, H, methyl-C, and methyl-H contributions. Twenty bands lying above the Fermi energy were considered in these calculations, along with a reasonable range of valence states. In regard to the accuracy of such calculations, we note that previous studies have found that the B3LYP method provides band gaps in good agreement with experimental values in a wide variety of materials, including molecular crystals,[37] elemental solids, semiconductors, and transition-metal compounds.[38]

III. Results and Discussion

i. Crystal Structure. Two previous publications have described the solid-state structure of phase I DMU;[17,19,20] we depict the geometries of the previously known and new phases in Figure 1b and c, respectively, alongside the phase I structure of urea for direct comparison (Figure 1a). As with phase I urea, both phases of DMU feature one-dimensional chains of molecules linked by hydrogen bonding along the *c*-vector. The difference between the two phases of DMU is, however, immediately apparent, with the phase II neighboring chains adopting alternating directions, leading to the nonpolar lattice that is characteristic of symmetrically disubstituted ureas, in general, and of urea phase I itself (Figure 1a). While for urea the neighboring chains are strictly perpendicular to one another with respect to the *a*,*b*-plane, this is not the case for DMU, where the angles between the chains drop to 70.2 and 89.6° for phases I and II, respectively. The addition of the methyl groups has reduced the overall interaction between molecules as hydrogen bonding in the *a*,*b*-plane is no longer possible, and as a consequence of this steric bulk, a neighboring molecule no longer sits directly above a carbonyl group. A comparison of the experimental and optimized first-principles geometries for both polymorphs is presented in Table 1. We see that the majority of the calculated structural parameters are consistent with the corresponding experimental values, showing maximum deviations of 2.5 and 1.5% of the latter values in phases I and II, respectively. However, poorer agreement with experiment is evident in the C−N−C−H dihedral angles and in the N−H bond lengths. The former deviations are likely due to the flatness of the potential energy surface for the rotation of the methyl groups, while the latter arise out of a combination of the usual difficulties encountered in locating H atoms in X-ray diffraction experiments with the fact that our calculations pertain only to the athermal limit.

ii. Relative Phase Stability. Complementing the X-ray diffraction results discussed above, first-principles calculations offer further insight into the energy scales governing polymorphism in this material and into the relative contribution of internal energy, vibrational enthalpy, and entropy to the free-energy difference separating the phases. We find that phase II is marginally more stable than phase I, but the difference in internal energies amounts to only 0.2 J mol^{-1}. Incorporating the zero-point vibrational contributions derived from the Γ-point optical modes increases the energy difference to 0.5 kJ mol^{-1}, while the inclusion of the thermal and entropic contributions at a temperature of 20 K leads to a free-energy difference of 0.4 kJ mol^{-1}. We note also that the work done due to the change in the molar volumes between the phases, $p\Delta V$, amounts to only 0.1 J mol^{-1} at atmospheric pressure, which may be safely neglected. Figure 2 presents the free-energy difference $\Delta G_{\mathrm{II-I}}$ separating the two phases for temperatures in the range from 20 to 400 K. While the difference in the stabilities remains marginal across the range, we see that there is a change of sign around 100 K, so that phase II is more stable below this value and phase I is more stable above. Taken together, the computed thermodynamical values support the suggestion that the phase II polymorph of DMU should be considered a readily accessible structure.

TABLE 1: Relevant Solid-State Calculated and Experimental Structural Parameters (*r*/Å, ∠/°) for DMU Phases I (*Fdd*2 space group) and II ($P2_12_12$ space group), Both with Local C_2 Molecular Symmetry

	phase I		phase II	
parameter	expt.[20]	calc.	expt.	calc.
C−O	1.242(4)	1.250	1.231(3)	1.249
C−N	1.329(11)	1.358	1.3428(19)	1.3589
N−CH_3	1.443(11)	1.451	1.432(3)	1.450
N−H	1.080(4)	1.016	0.8925(14)	1.0158
N···O′[a]	2.868(6)	2.841	2.891(2)	2.868
N−C−N	117.1(8)	115.8	116.36(19)	115.98
O−C−N−H	−175.4(9)	−179.9	−178.3(2)	−176.0
C−N−C−H	180.0(8)	163.8	175.0(2)	171.7

[a] O′ denotes an oxygen atom on a neighboring molecule.

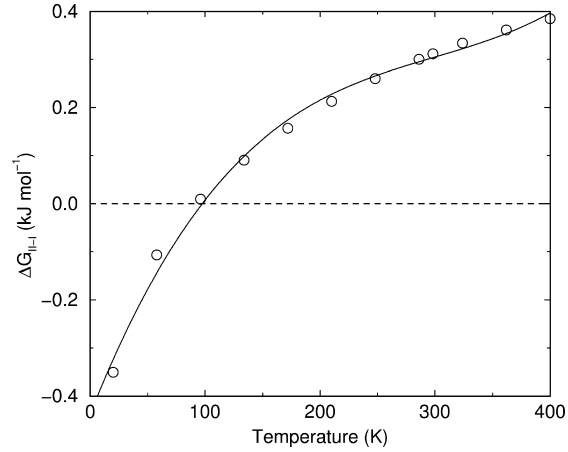

Figure 2. Plot of the variation of the difference, $\Delta G_{\mathrm{II-I}}$, in the Gibbs free energies of the polymorphs with temperature. Solid line shows a third-order polynomial fit to the data.

iii. Solid-State Vibrational Spectra. A comparison of the vibrational frequencies of both forms is of interest for any insight it may provide into the variations in intermolecular interaction strengths between the polymorphs. First-principles phonon calculations are of particular value in this regard, given that they often permit for the direct assignment of the modes obtained from experiment and can access modes that are silent or present

TABLE 2: Calculated Harmonic, Anharmonic, and Experimental[21,39] Frequencies (ω, cm^{-1}), Mode Assignments (IP indicates the in-phase FGS component and OP the out-of-phase component), Irreducible Representations (S), Factor Group Splittings (FGS, cm^{-1}), and Infrared and Raman Activities (a = active, i = inactive) of the Normal Modes of the Phase I DMU Crystal in the *Fdd*2 Space Group

ω_{harm}	ω_{anharm}	ω_{exp}	assignment[a]		S	FGS	IR	Raman
3468.7	3300.4	3357	ν_sN−H	OP	A_2	0.63	i	a
3454.8	3283.0	3335	ν_{as}N−H	IP	B_2	0.17	a	a
3130.8	3023.7	2994	$\nu_{as}CH_3$	IP	B_2	0.95	a	a
3130.4	3023.3	2994	ν_sCH_3	IP	A_1	0.12	a	a
3092.7	2985.6	2947	ν_sCH_3	OP	A_2	7.69	i	a
3088.3	2981.2	2947	$\nu_{as}CH_3$	OP	B_1	5.00	a	a
3035.7	2928.6	2904	ν_sCH_3	IP	A_1	2.40	a	a
3034.1	2927.0	2883	$\nu_{as}CH_3$	IP	B_2	4.95	a	a
1653.4		1621	νC−O	IP	A_1	3.08	a	a
1651.2		1595	δ_{as}N−H + ν_{as}C−N	IP	B_2	18.59	a	a
1589.8		1542	δ_sN−H	IP	A_1	0.64	a	a
1537.4		1480	$\delta_{as}CH_3$	OP	B_1	12.98	a	a
1530.5		1477	δ_sCH_3	OP	A_2	15.98	i	a
1509.2		1453	δ_sCH_3	OP	A_2	21.93	i	a
1503.2		1445	$\delta_{as}CH_3$	OP	B_1	14.87	a	a
1464.4		1438	$\delta_{as}CH_3$	IP	B_2	3.47	a	a
1458.3		1422	δ_sCH_3	IP	A_1	4.84	a	a
1311.0		1273	ν_{as}C−N + δ_{as}N−H	IP	B_2	5.63	a	a
1225.3		1176	ν_sN−R	OP	A_2	1.20	i	a
1206.9		1138	ρ_sCH_3	IP	A_1	1.67	a	a
1175.4		1195	$\rho_{as}CH_3$	IP	B_2	3.63	a	a
1163.7		1165	$\rho_{as}CH_3$	IP	B_2	1.57	a	a
1155.6		1117	ρ_sCH_3	OP	A_2	2.15	i	a
1061.4		1042	ν_{as}N−R	OP	B_1	5.44	a	a
955.9		933	ν_sC−N + ρ_sCH_3	OP	A_2	1.55	i	a
788.8		776	πC−O	OP	B_1	1.74	a	a
731.8		674	τ_{as}C−N	IP	B_2	14.86	a	a
702.7		704	δC−O + $\rho_{as}CH_3$	IP	B_2	3.87	a	a
625.8		505[b]	τ_sC−N	OP	A_2	7.24	i	a
511.2		508	δNCN	OP	A_2	1.78	i	a
346.7		351	δ_{as}N−R	IP	B_2	1.42	a	a
243.6		242	δ_sN−R	OP	A_2	1.34	i	a
169.1		199[b]	π_sN−H + τ_sC−N	IP	A_1	2.65	a	a
153.0		136	τ_{as}N−R	OP	B_1	1.86	a	a
138.9		132[b]	π_{as}N−H + τ_{as}N−R	IP	B_2	10.59	a	a
125.2		156[b]	τ_sN−R + π_sN−H	IP	A_1	22.85	a	a

[a] The attributed assignments correspond to the dominant motion at each frequency; where a mode comprises two or more component motions, they are presented in order of decreasing weight. Intermolecular symmetrically equivalent positions were found based on the operator $x + 1/4; -y + 1/4; z + 1/4$. R represents the methyl group. [b] Value calculated by Keuleers et al.[21]

TABLE 3: Calculated Harmonic and Anharmonic Frequencies (ω, cm^{-1}), Mode Assignments (IP indicates the in-phase FGS component and OP the out-of-phase component), Irreducible Representations (S), Factor Group Splittings (FGS, cm^{-1}), and Infrared and Raman Activities (a = active, i = inactive) of the Normal Modes of the Phase II DMU Crystal

ω_{harm}	ω_{anharm}	assignment[a]		S	FGS	IR	Raman
3480.9	3313.1	ν_sN−H	OP	B_1	1.53	a	a
3466.9	3297.2	ν_{as}N−H	OP	B_2	1.16	a	a
3147.1	3039.0	$\nu_{as}CH_3$	OP	B_2	3.59	a	a
3146.6	3038.5	ν_sCH_3	IP	A	3.08	i	a
3097.2	2989.1	$\nu_{as}CH_3$	OP	B_2	1.84	a	a
3095.3	2987.2	ν_sCH_3	OP	B_1	0.05	a	a
3039.9	2931.8	$\nu_{as}CH_3$	OP	B_2	5.63	a	a
3035.7	2927.6	ν_sCH_3	IP	A	1.53	i	a
1653.6		δ_{as}N−H + ν_{as}C−N	OP	B_2	26.90	a	a
1652.7		νC−O + δ_sN−H	OP	B_1	4.67	a	a
1584.8		δ_sN−H	OP	B_1	0.68	a	a
1536.1		$\delta_{as}CH_3$	IP	B_3	19.21	a	a
1534.7		δ_sCH_3	OP	B_1	18.48	a	a
1510.1		δ_sCH_3	OP	B_1	17.41	a	a
1496.3		$\delta_{as}CH_3$	IP	B_3	16.37	a	a
1471.5		$\delta_{as}CH_3$	IP	B_3	8.95	a	a
1464.2		δ_sCH_3	OP	B_1	3.45	a	a
1311.4		ν_{as}C−N + δ_{as}N−H	OP	B_2	7.80	a	a
1220.1		ν_sN−R	IP	A	0.89	i	a
1204.9		ρ_sCH_3 + νC−O	IP	A	0.74	i	a
1173.9		$\rho_{as}CH_3$	OP	B_2	6.57	a	a
1164.8		$\rho_{as}CH_3$	IP	B_3	7.60	a	a
1160.6		ρ_sCH_3	OP	B_1	7.77	a	a
1057.9		ν_{as}N−R	IP	B_3	6.24	a	a
953.6		ν_sC−N + ρ_sCH_3	OP	B_1	3.59	a	a
785.2		πC−O	IP	B_3	0.40	a	a
713.1		δC−O + τ_{as}C−N	OP	B_2	8.46	a	a
685.2		τ_{as}C−N + δC−O	OP	B_2	10.45	a	a
601.4		τ_sC−N	OP	B_1	4.92	a	a
514.7		δNCN	OP	B_1	2.46	a	a
346.7		δ_{as}N−R	OP	B_2	1.92	a	a
246.2		δ_sN−R	OP	B_1	1.28	a	a
184.7		π_sN−H	OP	B_1	10.59	a	a
159.9		τ_{as}N−R	OP	B_2	10.26	a	a
128.6		π_{as}N−H + τ_{as}N−R	IP	B_3	1.67	a	a
112.4		τ_sN−R	IP	A	3.98	i	a

[a] The attributed assignments correspond to the major component at each frequency; where there is strong coupling of modes, the component motions are presented in order of decreasing weight. Intermolecular symmetrically equivalent positions were found based on the operator $-x + 1/2; y + 1/2; -z$. R represents the methyl group.

with weak intensities in IR or Raman spectra. Here, the normal modes of each phase were obtained from lattice dynamics calculations performed subsequent to accurate geometry optimizations. The primitive cells of both polymorphs contain two molecules, and we therefore anticipate a total of 84 normal modes in each lattice. Three of these modes correspond to acoustic motions, the frequencies of which tend toward 0 at the Γ-point. Moreover, the presence of multiple molecules in the cell leads to the existence of modes composed of in-phase and out-of-phase combinations of near-identical intramolecular motions. The differences in the frequencies of such motions constitute the well-known Davydov or factor group splittings (FGS). Tables 2 and 3 contain the 36 frequencies computed for the intramolecular motions, along with the corresponding assignments, FGS values, irreducible representations, and infrared and Raman activities. The assignment of the modes is not straightforward and relies upon separate visualizations of the sets of atomic displacement patterns. Our assignments for phase I are compared with those reported by Keuleers et al.[21] A similar analysis is provided for the low-frequency modes in Table 4. However, strong coupling of the internal and external motions of the molecules renders the clear assignment of the latter modes difficult, and therefore, we report only their symmetries and IR and Raman activities.

The frequencies calculated for phase I DMU generally overestimate the experimental values,[21,39] but the average deviation amounts to less than 3%. It is worth reiterating that this accuracy is achieved without resorting to scaling. In the case of the four low-frequency modes for which no experimental frequencies were available, comparison was instead made with the values calculated by Keuleers et al.[21] The agreement between our solid-state frequencies and the values obtained from the earlier cluster calculations is less satisfactory. This is a reasonable finding given that the lack of experimental data in this

TABLE 4: Frequencies (ω, cm^{-1}), Irreducible Representations (S), and IR and Raman Activities (a = active, i = inactive) of the Low-Frequency Modes in Both Phases of DMU

Phase I				Phase II			
ω	S	IR	R	ω	S	IR	R
117.4	B_2	a	a	108.8	B_1	a	a
115.0	B_2	a	a	106.6	B_3	a	a
114.1	B_1	a	a	100.7	B_1	a	a
102.2	B_1	a	a	82.7	B_3	a	a
90.8	A_1	a	a	72.3	B_2	a	a
87.7	A_2	i	a	55.4	B_3	a	a
62.2	B_2	a	a	54.8	B_2	a	a
60.7	B_1	a	a	51.1	A	i	a
8.1	A_2	i	a	40.4	A	i	a

region hindered the cluster calculations, which relied upon scaling to achieve meaningful comparisons with the experimental data.

Turning now to discuss our assignments of the individual phase I modes, we find that the majority of these are in agreement with those made by Keuleers et al.[21] Notable differences emerge in just two cases. First, the mode at 704 cm^{-1}, which was previously assigned to δC−O, is now reclassified as δC−O coupled to $\rho_{as}CH_3$; second, the mode at 132 cm^{-1}, previously assigned to purely τ_{as}N−H also has significant τ_{as}N−R character. Keuleers and co-workers[21] also ranked the individual components of the motion in each mode by their potential energy contribution. We find for the modes that we calculated at 1509.2, 1464.4, 1225.3, 1206.9, 1163.7, 625.8, 153.0, and 138.9 cm^{-1} that the dominant components obtained from our calculations do not match those reported within the earlier study but were nevertheless present as one of the secondary components. Turning to discuss the anharmonic corrections computed for the high-frequency stretching modes, we find that these amount to −168 and −172 cm^{-1} for the symmetric and asymmetric N−H stretches, respectively, and −110 cm^{-1} for the symmetric C−H stretch. It was not possible to treat the various ν_{as}C−H motions separately, and therefore, the correction obtained for the totally symmetric mode was applied to all of the CH_3 stretching modes. The frequencies of the ν_s and ν_{as}N−H modes are overestimated by 112−120 cm^{-1} in the harmonic approximation, while application of the anharmonic corrections leads to underestimation of the experimental values by some 50−60 cm^{-1}. The latter discrepancies are likely due to inaccuracies in the energies obtained from the B3LYP functional for stretches of the N−H bonds beyond their equilibrium lengths. Indeed, previous studies have shown that an accurate representation of the donor proton stretching potential in hydrogen bonds requires the use of a hybrid functional containing a mixture of Fock exchange in excess of the 20% applied here.[40] Application of the anharmonic corrections to the various ν CH modes yields frequencies that overestimate experimental values by amounts in the range of 30−40 cm^{-1}. We conclude that the inclusion of anharmonicity in the donor proton stretching motions leads to improved agreement with experiment in all cases.

For comparison we obtained the solid-state Raman frequencies for phase II, but an overlay with those obtained for phase I over the range of 200−3600 cm^{-1} showed no appreciable differences within the resolution of the spectrometer (2 cm^{-1}). Turning now to the calculated values, we observed only very marginal differences between the frequencies and assignments of the normal modes in each phase, in keeping with the fact that the two structures differ only in the relative orientations of their hydrogen-bonded chains. The frequencies in which some deviations between the two phases do occur are the low-energy modes 713.1, 685.2, 601.4, 159.9, 128.6, and 112.4 cm^{-1}. These differences would often appear to be due to the fact that the modes occur in a different order in each phase (e.g., the δC−O and τ_{as}C−N modes have frequencies of 713.1 and 685.2 cm^{-1} respectively in phase II and 702.7 and 731.8 cm^{-1}, respectively, in phase I).

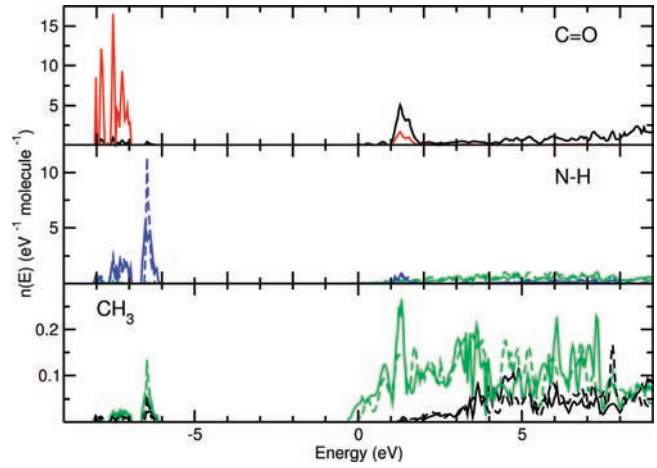

Figure 3. Plots of the variations in the atom-projected densities-of-states, $n(E)$, with energy in phases I (solid lines) and II (dashed lines) of DMU. Black, red, blue, and green lines correspond to C, O, N, and H contributions, respectively.

iv. Electronic Structure. The atom-projected densities-of-states (DOS) plots for both polymorphs are shown in Figure 3. It is immediately clear that the characters of the upper valence and lower conduction bands are very similar in both phases. The uppermost valence band in phase II is narrower and more sharply peaked than that of phase I, while the conduction band edge falls at a slightly lower energy in phase I. Taking these effects together, we find that the band gaps are of near-equal widths, at 5.71 (217 nm) and 6.14 eV (202 nm) in phases I and II, respectively. These values place the fundamental optical absorption of DMU close to the boundary between the UVC and far-UV spectral regions. We emphasize again that the reliability of the band gaps obtained from the B3LYP Hamiltonian has been established by calculations in a wide range of materials.[37,38] The atomic contributions to the valence band edge states are in the order N ≫ C > O > H ≈ me-C ≈ me-H in both phases, while similar analyses of the conduction band edges yield a relatively even mixture of C, O, me-H, and H states in the range from 0 to 1 eV, with much larger contributions in the order C > O > N > H ≈ me-H in the range from 1 to 2 eV.

Useful insights into the electronic structure of the solids are obtained from calculations on the isolated DMU molecule using the same basis set and Hamiltonian. The orbital energies and assignments are presented in Table 5, examination of which reveals that they are in general agreement with the results of the solid-state calculations. The LUMO is of particular interest for it consists of N−H σ-antibonding states, stabilized by bonding overlap orthogonal to the N−H bond vectors. We would expect that such an orbital would be destabilized by the hydrogen bonding present within the solid phases, which explains why there is no corresponding band in the DOS plots of Figure 3. Thus, the comparison of the isolated molecule and solid-state calculations allows us to conclude that the dominant excitation of the latter corresponds to the transfer of an electron from the N lone pair to the C═O π-antibonding states.

TABLE 5: The Energies (eV), Irreducible Representations within the C_2 Point Group, and Assignments of the Uppermost Orbitals Obtained from a B3LYP Calculation upon the Isolated DMU Molecule

orbital	irrep	energy	assignment
LUMO+1	B	+1.47	N pπ + C=O π-antibonding
LUMO	A	+0.71	N−H σ-antibonding
HOMO	A	−6.67	N pπ + small C−H σ
HOMO-1	B	−6.80	N pπ + O pπ
HOMO-2	B	−7.32	N pπ + O pπ

Finally, we obtain some insight into the intermolecular interaction strengths from an examination of the N−H and H···O Mulliken overlap populations, obtaining values of 0.680 and 0.082 e, respectively, in phase I and 0.682 and 0.086 e, respectively, in phase II. We therefore conclude that the covalent contribution to the hydrogen bond interactions is of a similar magnitude in both phases. Moreover, the fact that the Mulliken charges on the N, H, and O atoms are of similar sizes, at −0.460, +0.284, and −0.529 e, respectively, in phase I and −0.458, +0.278, and −0.531 e, respectively, in phase II, suggests that there is no appreciable difference in the electrostatic contribution to the hydrogen bond strengths in both forms.

IV. Conclusions

In summary, a new polymorph of *N*,*N*′-dimethylurea (DMU) which possesses many similarities in the crystal packing arrangement with the parent urea structure has been found, characterized, and compared with a previously known phase by means of an approach combining X-ray crystallography, Raman spectroscopy, and first-principles calculations. The new phase was initially obtained fortuitously by crystallization from phosphoric acid solution but was also identified in a sample of DMU obtained directly from the supplier.

The space group symmetry of the new phase suggests that it may possess interesting and technologically relevant NLO properties, and we encourage any further characterization of the material in this regard. The vibrational spectrum of phase I DMU obtained from first-principles lattice dynamics calculations in the reassigned *Fdd*2 space group is in excellent agreement with the previous experimental data, and only very marginal differences were apparent upon comparison with phase II. Moreover, the thermodynamics derived from the Γ-point vibrational modes indicate that the two phases possess similar free energies. The computed electronic densities-of-states plots indicate that there is little variation in either the energies or character of the excitations of DMU between the phases. Viewed in a wider context, the present work contributes to the number of successful studies of molecular solids in which a combined experimental and first-principles theoretical approach has been adopted.

Acknowledgment. We acknowledge the EPSRC for funding under Grant GR/T21615, and C.A.M. acknowledges the award of a University Research Fellowship by the Royal Society. This work has made use of the resources provided by the EaSTCHEM Research Computing Facility (http://www.eastchem.ac.uk/rcf), which is partially supported by the eDIKT initiative (http://www.edikt.org).

Supporting Information Available: Crystallographic data and additional experimental information. This material is available free of charge via the Internet at http://pubs.acs.org.

References and Notes

(1) Bernstein, J. *Polymorphism in Molecular Crystals*, IUCr Monographs on Crystallography; Clarendon Press: Oxford, U.K., 2002.
(2) Fabbiani, F. P. A.; Pulham, C. R. *Chem. Soc. Rev.* **2006**, *35*, 932.
(3) Kitaigorodsky, A. I. *Molecular Crystals and Molecules*; Academic Press: New York, 1973.
(4) Martins, D. M. S.; Middlemiss, D. S.; Pulham, C. R.; Wilson, C. C.; Weller, M. T.; Henry, P. F.; Shankland, N.; Shankland, K.; Marshall, W. G.; Ibberson, R. M.; Moggach, S.; Brunelli, M.; Morrison, C. A. *J. Am. Chem. Soc.* **2009**, *131*, 3884.
(5) Nguyen, K. L.; Frisic, T.; Day, G. M.; Gladden, L. F.; Jones, W. *Nat. Mater.* **2007**, *6*, 206.
(6) Munshi, P.; Skelton, B. W.; McKinnon, J. J.; Spackman, M. A. *CrystEngComm* **2008**, *10*, 197.
(7) Corbin, P. S.; Zimmerman, S. C.; Thiessen, P. A.; Hawryluk, N. A.; Murray, T. J. *J. Am. Chem. Soc.* **2001**, *123*, 10475.
(8) Zhao, X.; Chang, Y. L.; Lauher, J. W.; Fowler, F. W. *J. Am. Chem. Soc.* **1990**, *112*, 6627.
(9) Nguyen, T. L.; Fowler, F. W.; Lauher, J. W. *J. Am. Chem. Soc.* **2001**, *123*, 11057.
(10) Sklar, N.; Senko, M. E. *Acta Crystallogr.* **1961**, *14*, 716.
(11) Deshapande, S. V. *Acta Crystallogr., Sect. B* **1968**, *24*, 1396.
(12) Coiro, V. M.; Giacomello, P.; Giglio, E. *Acta Crystallogr., Sect. B* **1971**, *27*, 2112.
(13) Stankovic, S.; Andreetti, G. D. *Acta Crystallogr., Sect. B* **1978**, *34*, 3787.
(14) Coe, S.; Kane, J. J.; Nguyen, T. L.; Toledo, L. M.; Wininger, E.; Fowler, F. W.; Lauher, J. W. *J. Am. Chem. Soc.* **1997**, *119*, 86.
(15) Callahan, B. P.; Yuan, Y.; Wolfenden, R. *J. Am. Chem. Soc.* **2005**, *127*, 10828.
(16) Ganapathy, S. *Chem. Eng. World* **1998**, *33*, 110.
(17) Mark, H. *Ber. Dtsch. Chem. Ges.* **1924**, *57B*, 1820.
(18) Allen, F. H.; Motherwell, W. D. S. *Acta Crystallogr., Sect. B* **2002**, *58*, 407.
(19) Pérez-Folch, J.; Subirana, J. A.; Aymami, J. *J. Chem. Crystallogr.* **1997**, *27*, 367.
(20) Marsh, R. E. *Acta Crystallogr., Sect. B* **2004**, *60*, 252.
(21) Keuleers, R.; Desseyn, H. O.; Rousseeau, B.; Van Alsenoy, C. *J. Phys. Chem. A* **2000**, *104*, 5946.
(22) Becke, A. D. *J. Chem. Phys.* **1993**, *98*, 5648.
(23) Lee, C.; Yang, W.; Parr, R. G. *Phys. Rev. B* **1988**, *37*, 785.
(24) Koch, W.; Holthausen, M. C. *A Chemist's Guide to Density Functional Theory*; Wiley-VCH: New York, 2000.
(25) Pascale, F.; Zicovich-Wilson, C. M.; Lopez, F.; Civalleri, B.; Orlando, R.; Dovesi, R. *J. Comput. Chem.* **2004**, *25*, 888.
(26) Zicovich-Wilson, C. M.; Pascale, F.; Roetti, C.; Saunders, V. R.; Orlando, R.; Dovesi, R. *J. Comput. Chem.* **2004**, 25.
(27) *SAINT; SAINT Area-Detector Software Package*, v7.01A; Bruker-AXS: Madison, WI, 2003.
(28) Sheldrick, G. M. *SADABS; SADABS*, v2.04; University of Gottigen: Germany, 2001.
(29) Altomare, A.; Cascarano, G.; Giacovazzo, C.; Guagliardi, A. *J. Appl. Crystallogr.* **1993**, *26*, 343.
(30) Watkin, D. J.; Prout, C. K.; Carruthers, J. R.; Betteridge, P. W.; Cooper, R. I. *CRYSTALS*, 12 ed.; Chemical Crystallography Laboratory: Oxford, U.K., 2003.
(31) Dovesi, R.; Saunders, V. R.; Roetti, C.; Orlando, R.; Zicovich-Wilson, C. M.; Pascale, F.; Civalleri, B.; Doll, K.; Harrison, N. M.; Bush, I. J.; D'Arco, P.; Llunell, M. *CRYSTAL06*; University of Torino: Torino, Italy, 2006.
(32) Krishnan, R.; Binkley, J. S.; Seeger, R.; Pople, J. A. *J. Chem. Phys.* **1980**, *72*, 650.
(33) Monkhorst, H. J.; Pack, J. D. *Phys. Rev. B* **1976**, *13*, 5188.
(34) Tosoni, S.; Pascale, F.; Ugliengo, P.; Orlando, R.; Saunders, V. R.; Dovesi, R. *Mol. Phys.* **2005**, *103*, 2549.
(35) Ashcroft, N. W.; Mermin, N. D. *Solid State Physics*; Harcourt Brace College: Fort Worth, TX, 1976.
(36) Andersson, O.; Ross, R. G. *Int. J. Thermophys.* **1994**, *15*, 513.
(37) Perger, W. F. *Chem. Phys. Lett.* **2002**, *368*, 319.
(38) Muscat, J.; Wander, A.; Harrison, N. M. *Chem. Phys. Lett.* **2001**, *342*, 397.
(39) Mido, Y.; Hiromu, M. *Bull. Chem. Soc. Jpn.* **1969**, *42*, 3372.
(40) Poater, J.; Sola, M.; Duran, M.; Robles, J. *Phys. Chem. Chem. Phys.* **2002**, *4*, 722.

JP900141Q